EAI Endorsed Transactions
on Energy Web
Research Article EAI.EU

# Two-stage high-frequency switching power supply device design study

Lijuan Zhang[1,*]

[1]Department of Electrical Engineering, Jilin Technology College of Electronic Information, Jilin, 132021, China

## Abstract

The current volume and efficiency of high-frequency switching power supplies in power supply system cannot meet practical requirements. Therefore, a modular equipment was studied to optimize the design of PWM rectifiers and DC-DC converters, and corresponding control strategies were adopted. At the same time, experimental verification was performed. The experimental results show that before using the control, there are two large secondary voltage ripples in the PWM rectifier, with an amplitude of approximately 8 V; After using the control, the amplitude was approximately 1 V, a decrease of 87.5%. In addition, the DC-DC converter module may have fluctuations when it is lifted, but the amplitude of the voltage wave remains basically 62 A after steady state. In practical applications, the ripple is controlled at 1 V through the proposed control method, and the actual displayed current is a relatively standard sine wave with a low distortion rate. Meanwhile, compared with other methods, the efficiency of the studied method is as high as 89.110%. Overall, the control strategy proposed by the research institute can effectively control the front and rear modules in theory. In practical applications, it can effectively improve the power output and reduce the pollution in the power grid. It has high effectiveness and feasibility in practical industrial application.

**Keywords:** PWM rectifier; DC-DC converter; High frequency switching; Power supply unit

Received on 27 10 2023, accepted on 20 09 2024, published on 06 02 2025



doi: 10.4108/ew.4241

*Corresponding author. Email: zhanglijuan0510@163.com

## 1. Introduction

The increasing demand for industrial production has led to the development of rectifier circuits in DC power supplies, among which linear regulated power supply technology has rapidly developed due to its high stability accuracy and low output voltage ripple [1-2]. However, traditional linear power supplies have drawbacks such as large volume and bulky devices. The emergence of switching power supplies has effectively solved this problem, and the continuous development of technology has led to the development and innovation of high-frequency switching power supply devices towards high-frequency and integrated directions. Due to their easy capacity expansion, small size, high power density, low cost and good universality, modular devices are widely used in production and daily life. The working principle of high-frequency switching power supply is to first rectify and filter the three-phase power grid voltage to form DC power with certain pulsating components. Then, by controlling the high-frequency conduction and switching off the switching tube, the DC input voltage is converted into square-wave AC power with equal amplitude and unequal width. After rectification, the DC power required by the user is obtained [3-4]. By operating in a high-frequency state, the cost and volume of the device are much smaller than those in a power-frequency state. Compared with traditional linear power supplies, high-frequency switching power supplies reduce heat dissipation and improve overall efficiency [5]. However, there is currently limited research on the application of modular technology in high-frequency switching power supplies, and the design and control of subsequent DC-DC converters have not achieved the parallel connection of multiple modules. Therefore, the study utilized modular equipment and designed a two-stage high-frequency switching power supply device, aiming to optimize the front and rear modular equipment and strengthen the integrated development of high-frequency switching power supply devices.

## 2. Literature Review

In the electric age, electricity is becoming the lifeblood of the economy, directly affecting the quality and efficiency of industrial production [6]. In electric power high-frequency switching technology is developing towards high frequency, digitalization and integration with the development of semiconductor technology [7]. To improve the stability of high-frequency switching power supplies, Arunkumar et al. proposed a multi-bus DC microgrid structure integrated with a supercapacitor transient state power supply, which effectively improved the power quality and enhanced the smoothness [8]. Liao et al. found the optimal magnetic components for high-frequency switching power supplies under size constraints. To find the optimal magnetic components for high-frequency switching power supplies under size constraints, Liao et al. developed a variety of inductor arrangements to effectively reduce power losses [9]. Cvetanovic et al. developed a small-signal model for high-frequency switching power supply devices to enhance harmonic stability, thereby increasing the sampling frequency and achieving effective prediction [10]. Weitz et al. developed a small-signal model for high-frequency switching powe supplies to find direct-to-digital (DC-DC) converters for a specific range of high-frequency switching frequencies. (DC-DC) converter for a specific range of high frequency switching frequencies, the design process is described in detail to improve its peak efficiency [11]. Elluru et al. developed and designed a low-loss diode single-blade double-throw absorber switch to control the high-frequency switching circuit to reduce the conduction time [12]. Rajesh et al. used the bidirectional principle to improve the conversion efficiency of the DC-DC converter to improve the conversion efficiency of DC-DC converters, they optimized the DC-DC converter using the bi-directional principle to effectively reduce its load [13]. Li et al. proposed an RF signal detection system to improve the power quality of high-frequency switching power supply devices to effectively improve their performance [14].

In addition, Sreenivasulu et al. proposed junction less tri-gate for high frequency applications to reduce the power consumption of tri-gate, thus effectively reducing its losses [15]. Omijeh et al. analyzed for transformer and transformer less variable DC to reduce the noise of high frequency power switching, thus providing help to improve the transient response [16]. Neti et al. proposed a new topology for multilevel inverters in order to optimize A new topology of switched capacitor was proposed to optimize the multilevel inverter, thus effectively solving the voltage balancing problem at both ends of the high-frequency switched capacitor [17]. Zhao et al. proposed a new energy management strategy based on fuzzy in order to improve the efficiency of power utilization in high-frequency switched-mode power supplies, thus effectively reducing the power loss [18]. Rasulkhani et al. proposed a new voltage value for high frequency switching to reduce the switched capacitors and multilevel inverters to effectively improve the topology performance [19]. Chu et al. proposed a driver with high frequency response circuit to improve the light absorption performance of power plant devices, thus effectively improving the light absorption efficiency of the corresponding devices [20]. Takahashi et al. placed their information and communication device gold specifically to improve the converter density of high-frequency switching power supplies, thus effectively improving their switching frequency [21].

From the research of scholars at home and abroad, it can be found that there is currently limited research on the application of modular technology in high-frequency switching power supplies, and the design and control of

downstream DC-DC converters have not achieved the parallel connection of multiple modules. Therefore, the research integrates and optimizes the front-stage Pulse Width Modulation (PWM) rectifier with the subsequent DC-DC converter, and proposes corresponding control strategies to control the current ripple changes. The theoretical and practical methods are innovative, and have played a promoting role in the design of its parallel structure and high-frequency switching power supply device.

Table 1. Comparison of research work with previous work

| Number | Author | Contribute |
|---|---|---|
| [8] | Arunkumar et al. | Improved power quality and enhanced stability |
| [9] | Liao H et al. | Developed various inductor arrangements to effectively reduce power loss |
| [10] | Cvetanovic et al. | Developed a small signal model for high-frequency switching power supply devices, thereby increasing sampling frequency and achieving effective prediction |
| [11] | Weitz et al. | Effectively improving its peak efficiency |
| [12] | Elluru et al. | Effectively reducing diversion time |
| [13] | Rajesh et al. | Effectively reducing transformer load |
| [14] | Li et al. | Proposed a detection system for radio frequency signals to effectively improve its performance |
| [15] | Sreenivasulu et al. | Proposed a junction free triple gate for high-frequency applications, effectively reducing its losses |
| [16] | Omijeh et al. | Helped improve transient response |
| [17] | Netiet al. | Effectively solving the voltage balance problem at both ends of high-frequency switching capacitors |
| [18] | Zhao et al. | Effectively reducing the loss of electrical energy |
| [19] | Rasulkhani et al. | Effectively improving topology performance |
| [20] | Chu et al. | Effectively improving the light absorption efficiency of the corresponding device |
| [21] | Takahashi et al. | Place high-frequency switching power supply information communication equipment specifically to effectively increase its switching frequency |
| Research method | - | Strengthening the integrated development of high-frequency power supply switching devices has played a promoting role in the design of their parallel structures and high-frequency switching power supply devices |

## 3. Research on high-frequency switching power supply device based on two-stage type

### 3.1. Analysis of Front Stage PWM Rectifier for High Frequency Switching Power Supply Device

In response to the trend of high-frequency switching power supply technology toward intelligent integration, the research uses modular equipment to optimize the integration of PWM rectifiers and post-stage DC-DC converters. The topology and control technology of the power electronic converter is the key technology of the high-frequency switching power supply, and the stabilized DC side of the front stage is the basis of the whole switching power supply [22]. However, when the grid voltage is unbalanced, the transient active power of the fundamental wave generates two ripple pulsation voltages. It not only causes the AC filter inductor operating temperature rise and loss increase, but also directly affects the output voltage performance of the rear DC-DC stage [23]. Therefore, a three-phase PWM rectifier is selected to control the grid balance and to suppress the two generated harmonics by using appropriate control strategies. Compared to traditional three-phase non-controlled or phase-controlled rectifiers, three-phase PWM rectifiers can achieve numerous advantages such as system power factor correction and suppression of grid side harmonic currents. Since the three-phase PWM rectifier has good control performance and can better solve the harmonic problem on the grid-side, it has been well used in modern industrial and high-frequency switching power supplies. Its topology is shown in Figure 1 [24].

In Figure 1, S denotes the switch; C denotes the DC-side filter capacitor. As can be seen from the Figure 1, the PWM rectifier works by effectively controlling the switching elements so that the voltage at the input of the

bridge arm is a PWM-modulated pulse. At higher switching frequencies, the input voltage to the three-phase bridge arm is fundamental and higher harmonics. Since the input choke provides a filtering effect, it can buffer the reactive power generated by the bridge arm pulses to some extent, thus making the grid-side current sinusoidal. The DC-side capacitor is effective in filtering higher order harmonic components, reducing DC-side voltage pulsation and reducing the effect of DC-side fluctuations on the AC current. According to the knowledge of current system, when the grid is in a balanced state, the voltages of the three phases of abc will generate a circular rotating magnetic field within a certain range. However, if the grid voltage is not balanced, an elliptical magnetic field is formed [25]. abc three-phase loop equation is shown in equation (1).

$$\begin{cases} L\dfrac{di_a}{dt} + Ri_a = e_a - u_{ra} \\ L\dfrac{di_b}{dt} + Ri_b = e_b - u_{rb} \\ L\dfrac{di_c}{dt} + Ri_c = e_c - u_{rc} \end{cases} \tag{1}$$

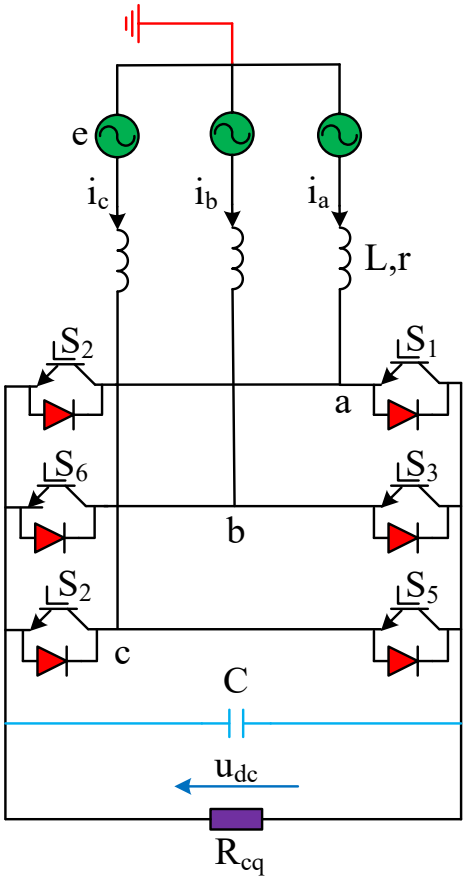


**Figure 1.** Topology diagram of three-phase PWM rectifier

In equation (1), $L$ represents the load current; $R$ represents the resistance; $r$ represents the equivalent resistance; $e_a$ , $e_b$ and $e_c$ represent the three-phase voltage at the access point of PWM rectifier; $i_a$ , $i_b$ and $i_c$ represent the three-phase current at the access point of PWM rectifier; $u$ represents the AC side voltage of the rectifier. According to Equation (1), when the voltage of the grid is unbalanced and only the fundamental component of the PWM rectifier is considered, the expression of the decomposition of the grid electric potential is shown in Equation (2).

$$\begin{bmatrix} e_a \\ e_b \\ e_c \end{bmatrix} = E_{m1}^{+} \begin{bmatrix} \cos(\omega t + \sigma_0) \\ \cos\left(\omega t - \dfrac{2\pi}{3} + \sigma_0\right) \\ \cos\left(\omega t + \dfrac{2\pi}{3} + \sigma_0\right) \end{bmatrix} + E_{m2}^{-} \begin{bmatrix} \cos(\omega t + \sigma_1) \\ \cos\left(\omega t + \dfrac{2\pi}{3} + \sigma_1\right) \\ \cos\left(\omega t - \dfrac{2\pi}{3} + \sigma_1\right) \end{bmatrix} + E_{m3}^{0} \begin{bmatrix} \cos(\omega t + \sigma_2) \\ \cos(\omega t + \sigma_2) \\ \cos(\omega t + \sigma_2) \end{bmatrix} \tag{2}$$

In equation (2), $E_{m1}^{+}$ , $E_{m2}^{-}$ and $E_{m3}^{0}$ represent the peak values of the positive, negative and zero sequence fundamental components, respectively; $\sigma_0$ , $\sigma_1$ and $\sigma_2$ represent the initial phase angles of the positive, negative and zero sequence components, respectively. It is worth noting that the grid-side input voltage of the three-phase PWM rectifier is usually connected into a Y-shape, so it does not produce zero-sequence current. The effect of the zero-sequence electric potential can be completely ignored under general circumstances. On this basis, when the voltage of the three-phase grid is in an unbalanced state and the sum of the three three-phase voltages is not zero, the expression is shown in equation (3).

$$u_{no}=\frac{1}{3}\left[e_a+e_b+e_c-u_{dc}\left(s_a+s_b+s_c\right)\right] \tag{3}$$

In equation (3), $u_{no}$ represents the measured voltage at unbalance; $s_a$ , $s_b$ and $s_c$ represent the three-phase switching functions. Therefore, when in the coordinate system of two-phase stationary αβ, the complex vector expression of the grid voltage is shown in equation (4).

$$E_{\alpha\beta}=\frac{2}{3}\left[e_a+e_b e^{j2\pi/3}+e_c e^{-j2\pi/3}\right] \tag{4}$$

In equation (4), $E_{\alpha\beta}$ represents the complex vector of the grid voltage; $j$ represents the inductance. From this, it can be found that when the grid voltage is in an unbalanced state, $E_{\alpha\beta}$ consists of the components of positive and negative sequence. Similarly, in two coordinate systems with the same step rotation, the expression of the complex vector of the grid voltage is shown in equation (5).

$$E_{\alpha\beta}=e^{j\omega t}E_{dq}^{+}+e^{-j\omega t}E_{dq}^{-} \tag{5}$$

In equation (5). $\omega$ denotes the angular frequency of the grid voltage; $t$ denotes the time; $E_{dq}^{+}$ and $E_{dq}^{-}$ denote the positive sequence and negative sequence vectors of the grid voltage, respectively, and the expressions of both are shown in equation (6).

$$\begin{cases}E_{dq}^{+}=E_d^{+}+jE_q^{+}\\ E_{dq}^{-}=E_d^{-}+jE_q^{-}\end{cases} \tag{6}$$

In equation (6), $E_d^{+}$ and $E_d^{-}$ represent the positive and negative sequence vectors of the $d$ axis; $E_q^{+}$ and $E_q^{-}$ represent the positive and negative sequence vectors of the $q$ axis. Based on equation (6), the grid current and AC input voltage can be similarly transformed as shown in equations (7) and (8).

$$\begin{cases}I_{\alpha\beta}=e^{j\omega t}I_{dq}^{+}+e^{-j\omega t}I_{dq}^{-}\\ I_{dq}^{+}=I_d^{+}+jI_q^{+}\\ I_{dq}^{-}=I_d^{-}+jI_q^{-}\end{cases} \tag{7}$$

In equation (7), $I$ represents the current of the grid.

$$\begin{cases}U_{\alpha\beta}=e^{j\omega t}U_{dq}^{+}+e^{-j\omega t}U_{dq}^{-}\\ U_{dq}^{+}=U_d^{+}+jU_q^{+}\\ U_{dq}^{-}=U_d^{-}+jU_q^{-}\end{cases} \tag{8}$$

In equation (8), $U$ denotes the AC input voltage. Therefore, the expression of the mathematical equation of the whole rectifier system in the coordinate system of αβ is shown in equation (9).

$$E_{\alpha\beta}-U_{\alpha\beta}=L\left(dI_{\alpha\beta}/dt\right)+rI_{\alpha\beta} \tag{9}$$

By combining equations (6) to (9), the equation expressions of the positive sequence and negative sequence vector model of the three-phase PWM rectifier in the $dq$ coordinate system can be obtained as shown in equation (10).

$$\begin{cases}U_{dq}^{+}=E_{dq}^{+}-L\dfrac{dI_{dq}^{+}}{dt}\pm j\omega LI_{dq}^{+}-rI_{dq}^{+}\\ U_{dq}^{-}=E_{dq}^{-}-L\dfrac{dI_{dq}^{-}}{dt}\pm j\omega LI_{dq}^{-}-rI_{dq}^{-}\end{cases} \tag{10}$$

Eventually, the expansion of equation (10) leads to the expression of the mathematical equation for the converter in positive and negative sequence rotation coordinates in the unbalanced state of the grid voltage, as shown in equation (11).

$$\begin{cases}U_d^P=E_d^P-L\dfrac{dI_d^P}{dt}+j\omega LI_d^P-rI_d^P\\ U_q^P=E_q^P-L\dfrac{dI_q^P}{dt}+j\omega LI_q^P-rI_q^P\\ U_d^N=E_d^N-L\dfrac{dI_d^N}{dt}+j\omega LI_d^N-rI_d^N\\ U_q^N=E_q^N-L\dfrac{dI_q^N}{dt}+j\omega LI_q^N-rI_q^N\end{cases} \tag{11}$$

In equation (11), $P$ denotes the power. In the three-phase PWM rectifier, the instantaneous active power and the instantaneous reactive power on the AC side both generate 2-fold pulses. The instantaneous active power of the three-phase PWM rectifier is the charging power of the capacitor on the DC side. Therefore, in the case of instantaneous active current pulsation, the capacitor voltage on the DC side will change by 2x frequency, resulting in a 100Hz fluctuation. In high-frequency switching power supplies, the undulation of the front-end DC-side voltage will directly affect the output efficiency of the subsequent DC-DC and needs to be suppressed [26]. Therefore, to achieve the control in the $dq$ coordinate system, it is necessary to achieve the separation of the positive and negative sequence components of the grid unbalance voltage. The study chose the signal delay method to achieve the extraction of the positive and negative sequence components, while the negative sequence current injection is used to control the DC side voltage. At this point, the study regulates the current by controlling the power, and it suppresses the fluctuation of the active power and drives it to zero, considering the high demand of the high-frequency switching power supply for the DC side voltage performance.

## 3.2. Analysis of Rear Stage DC-DC Phase-shifting Full Bridge Converter in High Frequency Switching Power Supply Device

In high-frequency switching power supplies, the topology would be preferred for practical high-power applications. Therefore, the phase-shifted full-bridge zero-voltage switching circuit (ZVS DC-DC) is introduced in this study. DC-DC is an electrical energy conversion circuit or electromechanical device that can convert a DC power source into a DC power source of different voltages. Its power range can be from a small battery to a large high voltage power source. The DC-DC converter includes isolation and non-isolation, and the parallel connection of its modules can greatly reduce the voltage and current stress of individual modules, and effectively reduce the heat dissipation of individual modules, greatly shortening the research and development cycle. The full bridge variable topology is a commonly used circuit topology in DC-DC converters, and the research on ZVS DC-DC is even more popular. ZVS DC-DC uses phase shifting control in the control of the switching tubes, this method is easy to implement and combined with soft switching technology to achieve constant frequency zero voltage switching, reducing switching losses and current and voltage stresses on the switches. The topology is shown in Figure 2 [27].

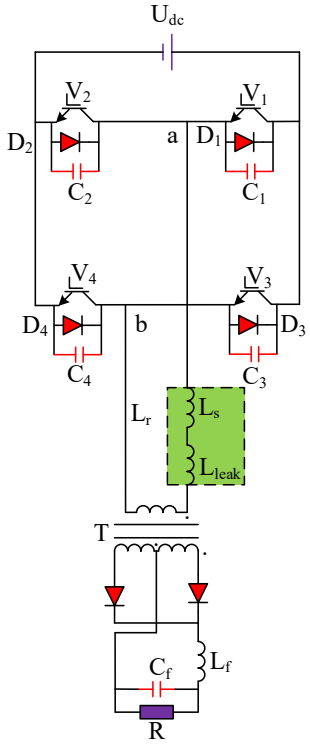


**Figure 2.** Topology of ZVS DC-DC

In Figure 2, CB indicates the blocking capacitor, whose function is to prevent the transformer from magnetic saturation; Ls indicates the inductor; T indicates the high-frequency voltager; D1~D4 indicates the internal parasitic diode; C1 ~C4 indicates the parasitic or external capacitor, whose function is to gradually increase the voltage across the switching tube at the turn-off point, so as to achieve zero-voltage shutdown and reduce the turn-off loss; DR1 and DR2 indicate the full-wave rectification; V1 ~V4 indicates the power tube drive waveform. According to the different switching states of the inverter bridge in one cycle, one switching cycle of the phase-shifting controlled ZVS DC-DC converter can be divided into 12 switching modes. The principle of the phase shift control is that V1 and V2 are alternately conducting, and V1 and V2 are opened before V3 and V4. Therefore, the bridge arm composed of the first two is called the leading bridge arm, while the bridge arm composed of the latter two is called the lagging bridge arm, and the leading phase is the phase shift angle. By controlling the magnitude of the phase shift angle, the conduction time of the switch tube is changed to adjust the output voltage. For the convenience of analysis, the following research ignores the conduction voltage drop of the tubes and diodes, and assumes that all power tubes, inductors, and capacitors are ideal components, that the resonance capacitors of the leading and trailing bridge arms are equal, and that the circuit filter inductance and isolation capacitance are sufficiently large.

At the moment when the switch tube V1 is turned off, due to the action of C1 and C2, the voltage at both ends of the switch tube cannot undergo sudden changes. Therefore

V1 is a zero voltage shutdown. In the resonance process of the leading bridge arm, the equivalent inductance involved in the resonance is large, so it can be equivalent to a constant current source. At a certain moment, when the voltage between two points is 0, the voltage of C2 also drops to 0, and the anti parallel diode D2 of V2 begins to conduct, thus ending the switching mode. The phase-shifted full-bridge circuit is actually a step-down converter circuit, but the presence of its leakage inductance causes a duty cycle loss problem. When the primary voltage waveform is a square wave, the secondary branch inductor keeps the secondary side refreshed, resulting in the primary side not being supplied to the output. In this case, the effective duty cycle expression is given by equation (12).

$$D_{eff} = D - \Delta D \tag{12}$$

In equation (12), $D_{eff}$ indicates the effective duty cycle, $D$ indicates the primary duty cycle, and $\Delta D$ indicates the lost duty cycle. The time occupied by the lost duty cycle is related to the input voltage and primary current. The higher the input voltage or the lower the primary current, the smaller the lost duty cycle. Therefore, the formula of $\Delta D$ is shown in equation (13).

$$\Delta D = \frac{t_{25}}{T_s/2} \tag{13}$$

In equation (13), $T_s$ denotes the moment. Therefore, the small signal perturbation formula for the effective duty cycle is shown in equation (14).

$$\hat{d}_{eff} = \hat{d}_i + \hat{d}_u + \hat{d}_d \tag{14}$$

In equation (14), $\hat{d}_{eff}$ indicates the small signal disturbance of effective duty cycle; $\hat{d}_i$ indicates the disturbance of output inductor current; $\hat{d}_u$ indicates the disturbance of output input voltage; $\hat{d}_d$ indicates the disturbance of duty cycle. The value of $\hat{d}_i$ is shown in equation (15).

$$\hat{d}_i = \frac{4L_r f_s}{n u_{dc}} \hat{i}_{L_f} \tag{15}$$

In equation (15), $L_r$ denotes the resonant inductance; $u_{dc}$ denotes the input voltage; $i_{L_f}$ denotes the secondary output current; and $n$ denotes the transformer ratio. For a parallel DC-DC system, an improved control strategy for autonomous current equalization is used to improve the current equalization characteristics. For a multi-module system, the voltages at both sides of the DC side remain almost constant when the system is in steady state. Therefore, as long as the input current balance is guaranteed, the output current balance can naturally be guaranteed. For the conventional current equalization control, the output current of each unit is fed into the voltage loop through the current equalization controller together with the current signal on the current equalization bus, and superimposed with the reference voltage signal to form a voltage command signal. It is modulated by the voltage inner loop controller to generate the output duty cycle signal. However, the bandwidth of the current compensation loop varies depending on the bandwidth of the voltage inner loop, making it unable to respond quickly to sudden load changes. With the conventional control method, the power supply has poor current equalization performance, which causes some modules to be subjected to high currents, thus increasing the difficulty of heat dissipation and possibly even exceeding the protection range of the system.

Therefore, in the study, the average current error from the output of the current compensation controller was superimposed with the current command signal from the voltage outer loop control to obtain the reference signal for the inner loop current. The control block diagram of the improved autonomous current averaging is shown in Figure 3.

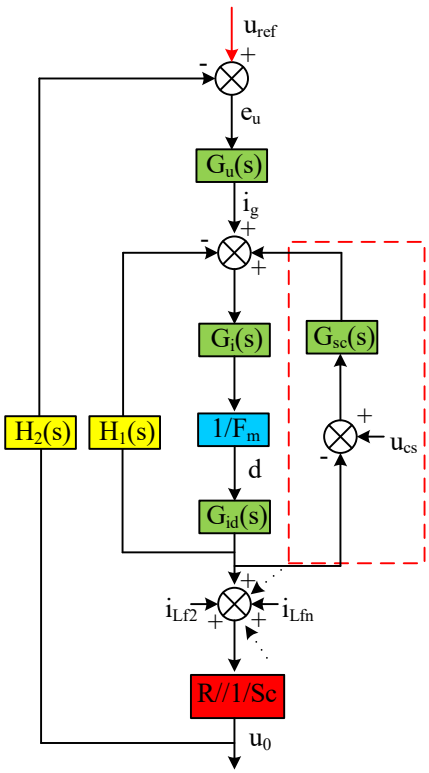


**Figure 3.** Control block diagram for improving independent current sharing

In Figure 3, Gu (s) represents the voltage compensation network; Gi (s) represents the current compensation network; Gsc (s) represents the open-loop transfer function of the current sharing loop; H2 (s) and H1 (s) represent the transfer functions of the output filter , which are set to 0.005 and 0.01; Gid (s) represents the transfer function of the duty cycle output voltage. From Figure 3, the study adds the current sharing error signal output by the current sharing controller to the current command signal output by the voltage outer loop controller to obtain a reference signal for the inner loop current. Based on the knowledge of power electronics, the diodes have unidirectional conductivity. Therefore, when the output current of each component is connected in parallel to the equalization bus, only the upper diode with the maximum current will be turned on. Since this module is automatic, the current signal on the equalization bus is the current of the master component. The rest of the slave components use the current signal of the master component as the required current equalization signal, and then adjust the output current of each component by the corresponding current equalization regulator, thus realizing automatic current equalization. To simplify the equalization controller design, the controller is selected as a proportional circuit. At the same time, the gain of the proportional link is increased in order to achieve a better response speed and to make the homogenization effect better. It should be noted that the bandwidth of the voltage and current loops needs to be considered to prevent system instability. After comprehensive analysis, the crossing frequency of the current inner loop is set to 2kHz, while the crossing frequency of the voltage outer loop is set to 200Hz. It should be ensured that the crossing frequency of the current sharing commutation is higher than that of the voltage loop and lower than that of the current inner loop. At the same time, in order to effectively control the output ripple current, the crossover frequency is set to a switching frequency of 1/4~1/5.

In addition, to solve the flux imbalance in the phase-shifted full bridge, the power switching tubes used in the study have a different storage time for one pair of tubes than for the other pair, resulting in an imbalance in the primary side volt-second, causing the core to be in saturation. When the transformer is saturated in the magnetic field, a large switching current is generated, which destroys the switching tubes and from this reduces the efficiency. To eliminate the DC component, it is common to use a straight capacitor in series with the primary side of the transformer. As the DC side flows through the isolation capacitor, a voltage drop occurs across the capacitor, causing a drop in the primary voltage, which usually cannot exceed 10% of the peak.

The normal working range of the high frequency switching power module is generally between -40℃ and 125℃, and the overtemperature protection point is set to 150℃. When a local short circuit occurs inside the system, the temperature on the load will rise rapidly. The device with temperature coefficient can be used to detect whether the chip is overheating, and the temperature change will cause the change of the current or voltage of the device. By comparing the signal at the temperature coefficient device with the reference signal, you can find out whether the system is overheating fault. The output signal of the overtemperature protection module is transmitted to the logic control unit, and the chip can be turned off in time when the circuit fails. Avoid damage to other modules and loads inside the system. The control flow of DC-DC converter is shown in Figure4. The DC-DC converter is responsible for the voltage adjustment at both ends of the supercapacitor, and switches the boost and buck modes in real time to achieve the purpose of matching the voltage of the supercapacitor and the voltage of the power battery. Therefore, it is necessary to properly control the DC-DC-converter, so as to accurately adjust the input and output voltage of the supercapacitor.

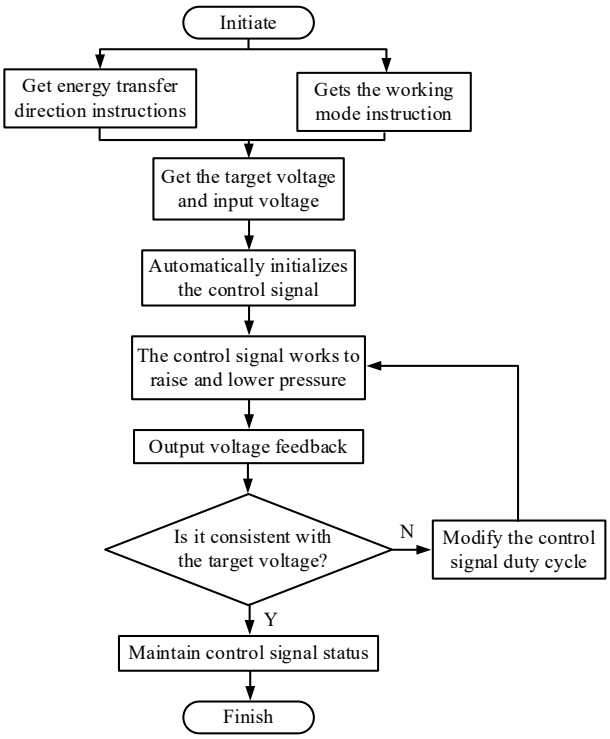


**Figure 4.** Control flow chart of DC-DC converter

## 4. Experimental analysis of two-stage high-frequency switching power supply device application

Before designing the two-stage high-frequency switching power supply device, the study was done in order to verify the effectiveness of the two control strategies and the corresponding experiments. The experimental setup is shown in Figure 5.

**Figure 5.** Schematic diagram of experimental equipment

From Figure 5, it can be seen that the device adopts a box structure, with a box size of 800 * 680 * 250mm. The box is divided into two layers, the upper layer is the main circuit board and control board, and the lower layer is the heat sink and output filter inductor. The layered structure design makes the device layout more compact and the device power density higher. A/D sampling circuit component with voltage signals ranging from -10V to+10V; The PWM level conversion circuit has an amplitude of 3.3V components, and the clamping circuit composed of diodes in reverse parallel clamps the amplitude of the AC input signal between -0.7V and+0.7V. In addition, the capacitance parameter in the experiment is 820 μ F. The withstand voltage is 450V, the rated collector voltage is 1700V, the rated current is 450A, the turn-on time delay is 0.21us, the turn-off time delay is 0.11us, the temperature in the switching state is -40~150 ℃, and the output filter inductance value is 0.5mH.

The temperature of the experimental environment should be controlled between 0℃ and 40℃. The normal working of the high frequency switching power module is affected by the temperature. An excessive temperature may deteriorate the performance or damage the device relative humidity should not exceed 90%, this is the requirement under the condition of 25℃±5℃. Figure6 shows the load change of the high-frequency switching power module, which changes the given voltage from 600V to 650V at 0.1s and recovers to 600V at 0.2s. It can be seen from Figure6 that no matter how the given voltage changes, the output voltage can be followed to the new command by about 0.025s. It shows that the improved sliding mode controller has good dynamic performance.

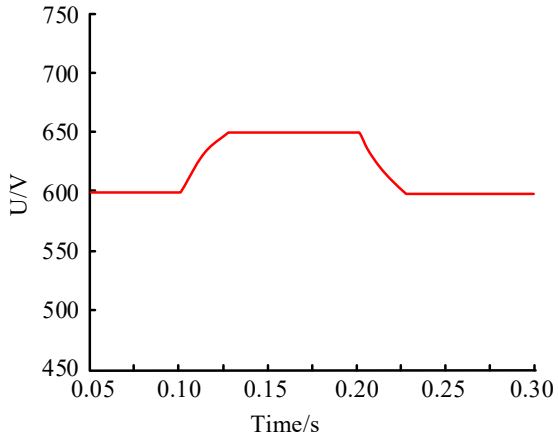


**Figure 6.** Load change of high-frequency switching power module

In order to actually simulate the unbalanced situation of the grid voltage, the PWM rectifier would rectify to supply the load before 0.5 s and at the three-phase balanced grid voltage; at 0.5 s, a set of three-phase

negative sequence voltages with an amplitude of 50V were injected. where the dynamic waveforms of the three-phase grid voltage and the change process of the DC-side voltage and the input three-phase AC without taking the balanced control method are shown in Figure 7.

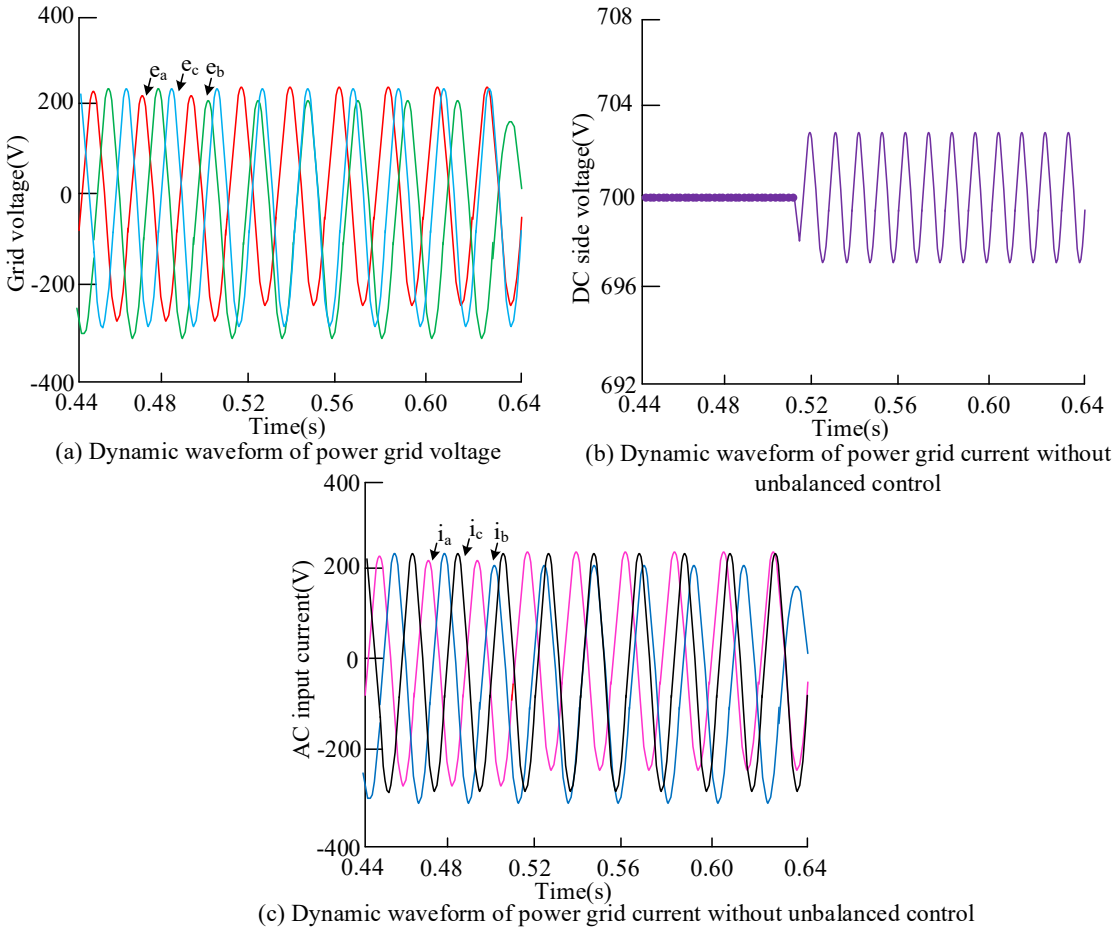


(a) Dynamic waveform of power grid voltage

(b) Dynamic waveform of power grid current without unbalanced control

(c) Dynamic waveform of power grid current without unbalanced control

**Figure 7.** Dynamic waveform of three-phase power grid voltage and the result without adopting balance control method

From Figure 7(a), it can be seen that the dynamic waveform of the original three-phase grid voltage varies up and down, and changes very frequently within 0.2s, with values generally ranging from -300V to 300V. From Figure 7(b), it can be seen that the dynamic waveform of the grid current without unbalance control is bounded at about 0.495s. Before this moment, the voltage on the DC side remains constant at 700V; after that moment the instrument shows fluctuations and is clearly different from the former, remaining between 692V and 708V. From Figure 7(c), it can be seen that the dynamic waveform of the grid with your stay without taking unbalance control is similar to the original dynamic waveform, with the difference that the value is smaller and maintained between -200V and 200V. Based on this, the study added the control method selected for the study to analyze its DC side voltage and AC input current, respectively, and the results are shown in Figure 8.

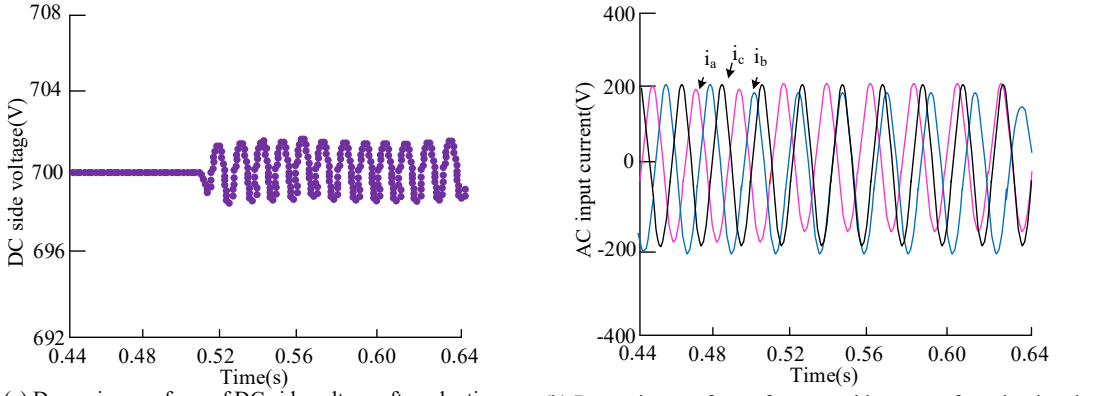


(a) Dynamic waveform of DC side voltage after adopting the control method in this paper

(b) Dynamic waveform of power grid current after adopting the control method in this paper

**Figure 8.** Analysis results of DC side voltage and AC input current

From Figure 8(a), it can be seen that with the control method given in the study, the amplitude of the DC-side voltage changes much less after 0.5s, roughly around 1V, which is 87.5% lower. It can be seen from Figure 8(b) that the simulated dynamic waveform is similar to the original waveform, and the degree of change is basically the same. Combining Figure 7 and Figure 8, it can be found that the control method selected in the study effectively improves the quality of the DC side voltage, while the addition of an appropriate negative sequence current on the network side also satisfies the voltage control requirements, so that the DC side voltage fluctuations are effectively suppressed. It also effectively ensures the output quality of the subsequent DC-DC power, thus ensuring the effectiveness of the overall high-frequency switching power supply device. On the basis of ensuring the effectiveness of the front-stage PWM rectifier, the study conducts simulation experiments on the rationality of the control method related to the rear-stage DC-DDC converter. The high-frequency switching frequency is set to 10 kHz before the experiment, and the simulated waveforms of the collector voltage and drive voltage waveforms of the switching tubes are shown in Figure 9.

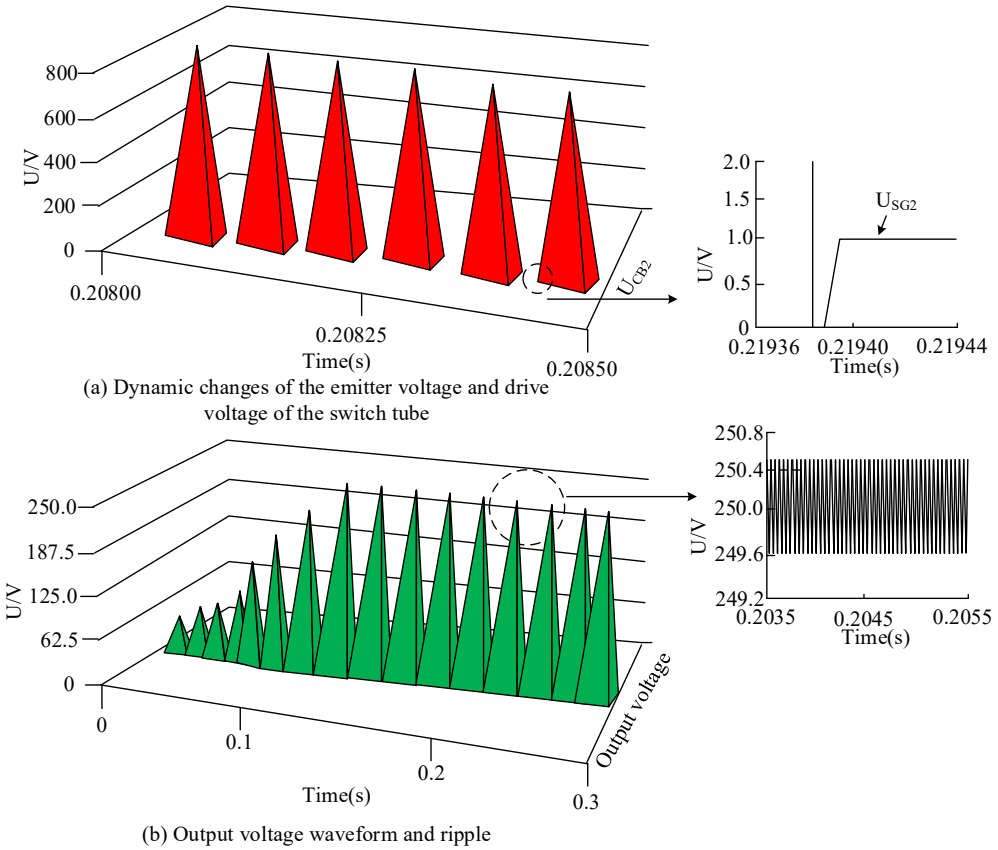


(a) Dynamic changes of the emitter voltage and drive voltage of the switch tube

(b) Output voltage waveform and ripple

**Figure 9.** Simulation results of collector emitter voltage and drive voltage waveform of switch

From Figure 9(a), it can be seen that a switching tube is turned on after its collector voltage drops to zero and its anti-parallel diode is turned on. And in the off state, zero voltage turn-off is achieved due to the presence of shunt or junction capacitance. Figure 9(b) gives the output waveform of 250 V. This waveform is around ±0.5 V, which has a good voltage regulation performance and meets the system requirements. Based on the single simulation module in Figure 9, in order to verify the effectiveness of the improved autonomous equalization control proposed in the study, the study again paralleled a sub-module with the same structure and ensured that the parameters, except for the output filter inductor, remained the same. The results are shown in Figure10.

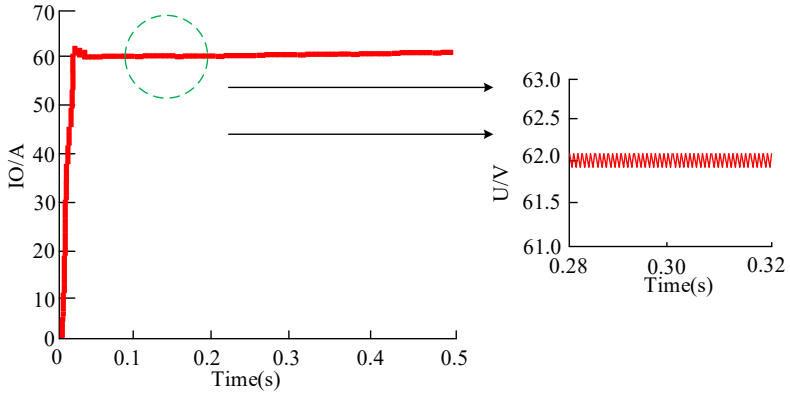


**Figure 10.** Current dynamic variation and steady state results of two modules

Figure 10 shows the current dynamics of the two modules. It is obvious from the Figure10 that there are some fluctuations in the current waveform in the rising section, and a little oscillation occurs. After the steady state, the value starts to appear stable and basically stays around 62A. The current ripple is also relatively small, with an amplitude of no more than 1A.

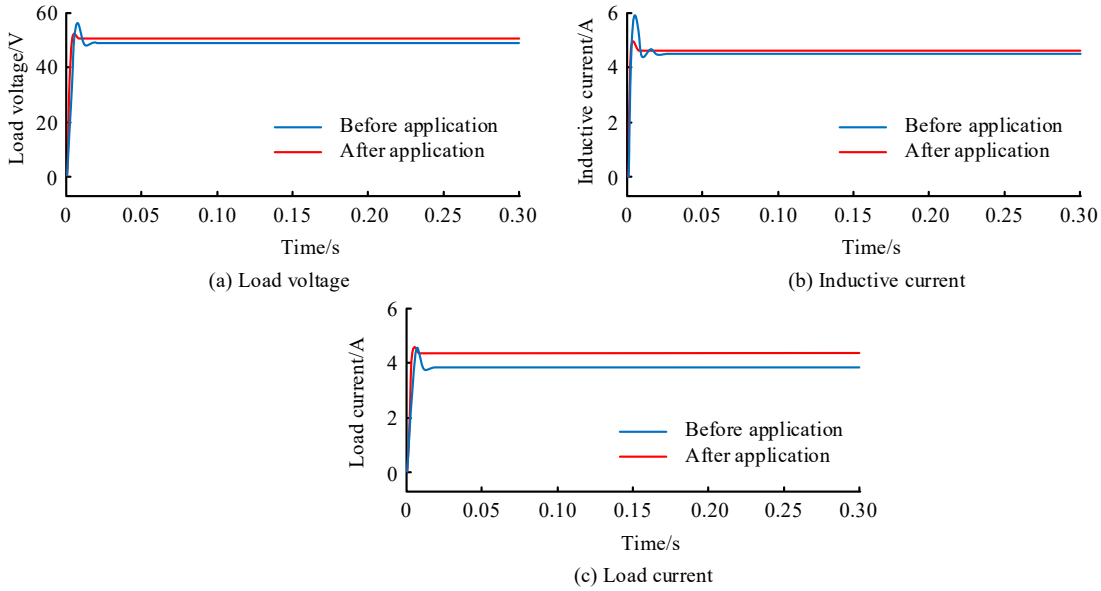


**Figure 11.** Simulation of transient response times before and after applying the control method

The transient response time before and after the application of the control method is simulated. The given DC input voltage is set to 100V and the reference voltage to 50V. The simulation results are shown in Figure11. It can be seen from the simulation results that before the control method proposed by the research institute, the control system had obvious oscillations during startup, and the overshot voltage was about 7.85V (15.7%), the system rise time was 2.88ms, and the adjustment time was 7.87ms. Therefore, the transient response time of the control system before the proposed control method is high, and the dynamic performance is not good enough. After the control method was proposed in the applied research institute, the overshoot of the control system at

startup was about 3.7% (1.86V), the rise time was 2.40ms, and the adjustment time was 5.37ms. In steady state, the output voltage and current hardly fluctuate. The above results show that the transient response time of the control system after the proposed control method is low, and the dynamic and static characteristics are improved to some extent. To further check the robustness and dynamic response characteristics of the system in combination with a load disturbance, the load changes from 2Ω to 4Ω in 0.3 s. The current results for both components are shown in Figure 12.

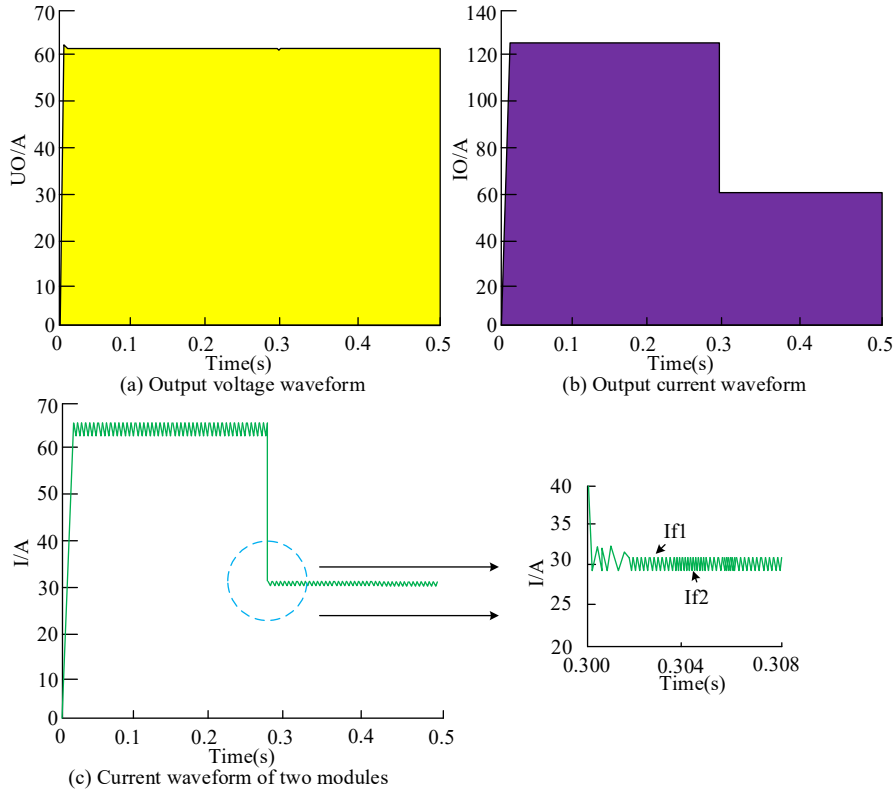


**Figure 12.** Current results for both components

The comprehensive Figure 12 shows that when the voltage of both components changes, the output voltage of both components shows a certain offset, but soon returns to the steady state, which also illustrates the equalization effect of the two parallel components from a different perspective, and also verifies the effectiveness of the equalization control method given in the study. Therefore, in order to verify the effectiveness of the overall control strategy on a real high-frequency switching power supply device, the study applied it to an experimental machine. Among them, the experimental results of the primary and secondary side voltages are shown in Table 2. As can be seen in Table 2, the output voltage on the primary side of the transformer shows a good square wave, and the peak on the secondary side of the transformer is almost twice as high. While the DC side voltage is less than 700 V (the DC side front voltage gradually increases during commissioning), the secondary side peak is likely to destroy the rectifier diode. This is because in high frequency, high power isolated DC-DC converters, the parasitic inductance and transformer leakage will cause the junction capacitance of the rectifier diode to resonate when the reverse recovery occurs, making the rectifier diode to experience reverse peak voltage and parasitic oscillation when it is turned off. With the addition of a parallel RC absorption circuit, the voltage spike voltage is well suppressed, greatly reducing the risk of diode breakdown.

Table 2. Original and secondary side voltage test results

| - | | Value | Average value | Minimum value | Maximum | Standard deviation |
|---|---|---|---|---|---|---|
| Waveform of primary output voltage | Spike voltage | 418.000V | 418.000 | 418.000 | 418.000 | 0.000 |
| | Frequency | 9.993kHz | 9.993k | 9.993k | 9.993k | 0.000 |
| Secondary output voltage waveform | Spike voltage | 904.000V | 627.000 | 72.000 | 912.000 | 402.000 |
| | Frequency | 10.110 kHz | 58.570M | 10.070k | 454.500M | 130.700M |
| Secondary voltage without RC | Spike voltage | 652.000V | 652.000 | 652.000 | 652.000 | 0.000 |
| Secondary side voltage with RC | Spike voltage | 792.000V | 792.000 | 792.000 | 792.000 | 0.000 |

Finally, the output voltage and the experimental waveform of the high-frequency switching power supply are shown in Figure 13.

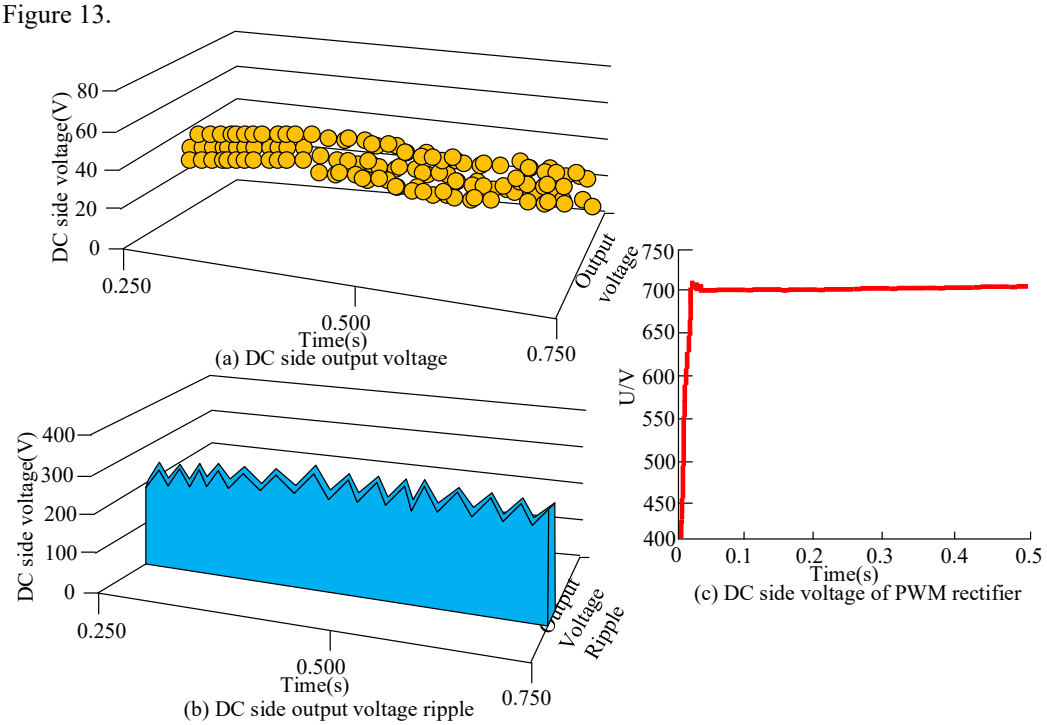


**Figure 13.** Experimental waveforms of output voltage and high-frequency switching power supply

From Figure 13(a), it can be seen that with the control strategy given in the study, the DC side voltage can be guaranteed to be stable at about 200V, while the control ripple is about 1V, which can meet the actual industrial needs. It can be seen from Figure 13(b) that the DC side capacitor voltage rises relatively quickly and can be stabilized smoothly at about 700V, which is a good control effect. In summary, the high-frequency switching power supply device constructed by the study is capable of efficiently outputting the DC power required by the industry. At the same time, the power factor of the whole device is relatively high, which reduces the burden on the power grid, and it is easy to achieve capacity expansion. In addition, the results of Table 2 and Figure 13 together show that the control strategy given in the study has effectiveness and feasibility.

Table 3. Efficiency and Output Stability Verification of Three Methods

| - | Input voltage | Power factor | Efficiency | Ideal output voltage | Measured output voltage | Core loss | Winding loss | Conduction loss |
|---|---|---|---|---|---|---|---|---|
| Research method | 176.000V | 0.987 | 89.110% | 80.000V | 80.250V | 4.990W | 18.220W | 21.360W |
| D | 176.000V | 0.987 | 87.660% | 80.000V | 81.010V | 9.170W | 25.500W | 33.210W |
| F | 176.000V | 0.987 | 85.620% | 80.000V | 80.980V | 14.690W | 35.690W | 29.410W |

To further validate the effectiveness of the control strategy proposed in the study, a comparison was made between the single stage forward power factor correction method (D) and the parallel promoted active power factor correction method (F) in terms of output efficiency and stability. The results are shown in Table 3.

The loss characteristics of iron core with ferrite as the main material are analyzed by loss separation method. The eddy current loss of high frequency transformer winding is analyzed by three-dimensional nonlinear time-harmonic field analysis method. In switching power supply, metal-oxide-semiconductor field effect tube and diode are the main factors causing power consumption, so the conduction loss of circuit part is calculated by the on-resistance of metal-oxide-semiconductor field effect tube and the forward conduction voltmeter of diode. From Table 3, it can be seen that the actual efficiency of the research method is as high as 89.110, which is higher than that of the comparison method. The core loss, winding loss and conduction loss are 4.990W, 18.220W and 21.360W respectively, which are lower than the comparison method. At the same time, the measured output voltage is 80.250V, with an error of only 0.25V. Overall, the high-frequency switching power supply device under the control strategy proposed in the study has high efficiency and stability.

## 5. Conclusion

To cope with the demand for intelligent integration of high-frequency switching power supplies, the study uses modular technology to optimize the design of the two-stage module before and after high-frequency switching. The corresponding control strategy is also proposed, and simultaneously analyzed through experiments. The experimental results show that, in the PWM regulator control strategy verification experiment, there are two large secondary voltage ripples with an amplitude of about 8V on the DC side before the control is introduced. After the control is introduced, it is effectively suppressed, with an amplitude of about 1V, which is reduced by about 87.5%. In the DC-DC converter control strategy verification experiment, the current waveform of the module oscillates in the rising phase, but is basically stable at about 62A after steady state, and the current ripple is also small. In the actual high-frequency switching power supply device, the DC side voltage is stabilized at 200 V and the ripple is controlled at 1 V. At the same time, the actual presented current exhibits a more standard sine wave with very small distortion rate. The DC side capacitor voltage is also stabilized at 700 V, showing a good control effect. Overall, the control strategy proposed in the study can effectively control the current fluctuations in both the front and rear modules. Under its control, the high-frequency switching power supply device can efficiently output DC power and reduce grid pollution. At the same time, the control strategy also demonstrates a high degree of effectiveness and feasibility, which can improve the stability of the output inductance current of the high-frequency power supply device. Because the high frequency and high voltage power supply has a small burn-through current, the overall output power is not very high, and it will be limited in applications requiring large burn-through current and high power. In the future, we can improve the circuit structure and the selection of components to make the output current larger. At the same time, the capacitor and discharge switches used to generate shock high voltage can be integrated into the same box, which can further improve the overall integration and portability of the power supply, and reduce the trouble of wiring.

## 6. Findings

The research is supported by Scientific Research Project of Jilin Provincial Department of Education in 2023, Research and Implementation of High Frequency Power Module, (No. JJKH20231012KJ).

## References

[1] Mukherjee S, Yousefzadeh V, Sepahvand A, Doshi M, Maksimović D. A two-stage automotive LED driver with multiple outputs. IEEE Transactions on Power Electronics, 2021, 36(12): 14175-14186.

[2] Wang J, Rasekh N, Yuan X, Dagan K J. An analytical method for fast calculation of inductor operating space for high-frequency core loss estimation in two-level and three-level PWM converters. IEEE Transactions on Industry Applications, 2020, 57(1): 650-663.

[3] Khatua S, Kastha D, Kapat S. A dual active bridge derived hybrid switched capacitor converter based two-stage 48 V

VRM. IEEE Transactions on Power Electronics, 2020, 36(7): 7986-7999.
[4] Goyal V K, Shukla A. Two-stage hybrid isolated dc–dc boost converter for high power and wide input voltage range applications. IEEE Transactions on Industrial Electronics, 2021, 69(7): 6751-6763.
[5] Zeng X, Yang Z, Wu P, Cao L, Luo Y. Power source based on electric field energy harvesting for monitoring devices of high-voltage transmission line. IEEE Transactions on Industrial Electronics, 2020, 68(8): 7083-7092.
[6] Qanbari T, Tousi B. Single-source three-phase multilevel inverter assembled by three-phase two-level inverter and two single-phase cascaded H-bridge inverters. IEEE Transactions on Power Electronics, 2020, 36(5): 5204-5212.
[7] Kopacz R, Harasimczuk M, Trochimiuk P, Wrona G, Rąbkowski J. Medium voltage flying capacitor DC–DC converter with high-frequency TCM-Q2L control. IEEE Transactions on Power Electronics, 2021, 37(4): 4233-4248.
[8] Arunkumar C R, Manthati U B, Punna S. Supercapacitor-based transient power supply for DC microgrid applications. Electrical Engineering, 2022, 104(2): 463-472.
[9] Liao H, Chen J F. Design process of high - frequency inductor with multiple air - gaps in the dimensional limitation. The Journal of Engineering, 2022, 2022(1): 16-33.
[10] Cvetanovic R, Petric I Z, Mattavelli P, Buso S. Accurate High-Frequency Modeling of the Input Admittance of PWM Grid-Connected VSCs. IEEE Transactions on Power Electronics, 2022, 37(9): 10534-10545.
[11] Weitz N, Utzelmann S, Ditze S, März M. A Resonant Push-Pull DC-DC Converter with an Intrinsic Current Source Behavior for Radio Frequency Power Conversion. IEEE Transactions on Power Electronics, 2022, 37(6): 7001-7012.
[12] Elluru D N, Awasthi A K, Gogineni S P, Taylor D, Shahabi A, Lemmon A N. Design of an Absorptive High-Power PIN Diode Switch for an Ultra-Wideband Radar. IEEE Journal of Microwaves, 2022, 2(2): 286-296.
[13] Rajesh P, Shajin F H, Kommula B N. An efficient integration and control approach to increase the conversion efficiency of high-current low-voltage DC/DC converter. Energy Systems, 2022, 13(4): 939-958.
[14] Li Z L, Xi X C, Chu H Y, Xu L Y, Gao Q, Zhao W S. Improving RT-WEDM performance with a radio frequency signal monitoring system. The International Journal of Advanced Manufacturing Technology, 2022, 118(1): 391-404.
[15] Sreenivasulu V B, Narendar V. A comprehensive analysis of Junctionless tri-gate (TG) FinFET towards low-power and high-frequency applications at 5-nm gate length. silicon, 2022, 14(5): 2009-2021.
[16] Omijeh B O, Onyekachukwu N, Nwachukwu P O. Comparative Analysis of Transformer and Transformer Less-Based Variable DC Power Supply. International Journal of Modern Engineering Research (IJMER), 2013, 3(1): 551-563.
[17] Neti S S, Anand V, Singh V. Single-Phase Generalized Switched-Capacitor Multilevel Inverter Using Reduced Number of Power Semiconductor Components with Voltage Boosting Ability. Arabian Journal for Science and Engineering, 2022, 47(3): 2613-2627.
[18] Zhao, Z H. Improved fuzzy logic control-based energy management strategy for hybrid power system of FC/PV/battery/SC on tourist ship. International Journal of Hydrogen Energy, 2022, 47(16): 9719-9734.
[19] Rasulkhani A, Taheri A. Multilevel Inverter based on switched-capacitor with reduced component count. International Journal of Electronics, 2022, 109(2): 200-220.
[20] Chu X, Liu J, Xun T, Wang L, Yang H, He J, Zhang J. MHz Repetition Frequency, Hundreds Kilowatt, and Sub-Nanosecond Agile Pulse Generation Based on Linear 4H-SiC Photoconductive Semiconductor. IEEE Transactions on Electron Devices, 2022, 69(2): 597-603.
[21] Takahashi S, Wada K, Ayano H, et al. Review of modeling and suppression techniques for electromagnetic interference in power conversion systems. IEEJ Journal of Industry Applications, 2022, 11(1): 7-19.
[22] Blaabjerg F, Yang Y, Kim K A, Rodriguez J. Power electronics technology for large-scale renewable energy generation. Proceedings of the IEEE, 2023, 111(4): 335-355.
[23] Mousavi S M J, Babaei E, Sabahi M, Komurcugil H. A Class of Bidirectional Single-Phase Z-Source AC–AC Converter with Continuous Input Current and Reduced Component Count. IEEE Transactions on Power Electronics, 2023, 38(5): 6311-6318.
[24] Mumtaz F, Yahaya N Z, Meraj S T, Singh B, Kannan R, Ibrahim O. Review on non-isolated DC-DC converters and their control techniques for renewable energy applications. Ain Shams Engineering Journal, 2021, 12(4): 3747-3763.
[25] Mukherjee S, Barbosa P. Design and Optimization of an Integrated Resonant Inductor with High-Frequency Transformer for Wide Gain Range DC–DC Resonant Converters in Electric Vehicle Charging Applications. IEEE Transactions on Power Electronics, 2023, 38(5): 6380-6394.
[26] Chien W, Chiu C C, Chen P H, Zhuo, J X, Hao J, Tsai C L. Reducing Surge Voltage and Ringing Effect of DC Voltage Converter by Transient Suppressor. Sensors and Materials, 2023, 35(7): 2413-2432.
[27] Yao H, Yan Y, Shi T, Zhang G, Wang Z, Xia C. A novel SVPWM scheme for field-oriented vector-controlled PMSM drive system fed by cascaded H-bridge inverter. IEEE Transactions on Power Electronics, 2021, 36(8): 8988-9000.